

COMET GIACOBINI-ZINNER DIAGNOSIS FROM RADIO MEASUREMENTS

N. Meyer-Vernet

CNRS UA 364, Observatoire de Paris, 92195 Meudon, Principal
Cedex, France

ABSTRACT

The physics of using a radioastronomy receiver as an in-situ detector of plasma, and in some cases of molecules and dust grains is reviewed, and applied to ICE encounter with comet Giacobini-Zinner. In the comet's plasma tail, the receiver recorded mostly quasi-thermal plasma noise. The spectroscopy of that noise yields the density and temperature of the main (cold) electron population, and parameters of hot electrons. The absence of grain detection yields a quantitative upper limit on grain mass or flux. An additional diagnosis is provided by partial occultations of both the radio galactic noise and the terrestrial kilometric radiation. Implications for comparison with earth-based measurements are indicated.

INTRODUCTION

On 11 September 1985, the ICE spacecraft passed 7800 km down the tail of comet Giacobini-Zinner, at ~ 21 km/s relative velocity. The radio astronomy receiver on board, which had been initially designed to track solar radioemissions /1/, provided an accurate diagnosis of the plasma electrons in the comet's tail and gave also an upper limit of dust mass or flux /2,3/.

This performance was made possible because the antennas and receiver were, by chance, ideally suited to allow spectroscopy of the plasma thermal noise in the quiet cold and dense comet's tail. This plasma diagnosis proved complementary of the more conventional plasma analyser /4/, which was suited for measuring the solar wind plasma but not the colder and denser cometary one.

The ICE radioastronomy experiment measures the electric field power spectrum at frequencies between 30 kHz and 2 MHz with two antennas (Figure 1) : (1) a dipole, made of two thin long wires 90 m tip-to-tip (perpendicular to the spin axis) ; (2) a monopole made of one thick short boom (parallel to the spin axis) mounted such that the receiver measures the voltage between the boom and the spacecraft. We show in the next Section that this configuration is very interesting : the long dipole is mainly sensitive to the thermal noise of the ambient plasma and is not perturbed by the spacecraft floating potential or proper sheath ; the monopole detects mainly the noise due to plasma particles impacts on (or photoelectron emission from) the spacecraft. Both can detect molecules or dust impacts on respectively the dipoles (1) or the spacecraft (2) whenever the impact rate and velocity are sufficient to generate appreciable secondary charged particles emission.

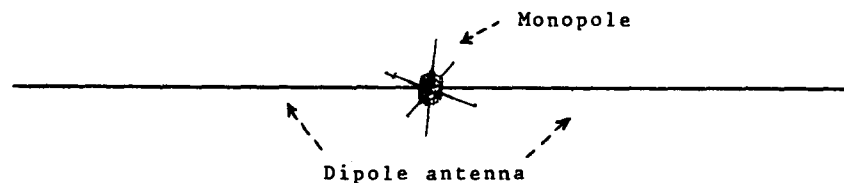


Fig. 1. Sketch of the radio astronomy antennas on the ICE spacecraft, roughly on scale, showing the huge extension of the dipole antenna with respect to other scalelengths.

Over more than 20000 km on each side of the point of closest approach to the comet, the dipole detected mainly the plasma thermal noise (Figure 3). The spectroscopy of that noise allowed to obtain the cometary electron parameters and provided an upper limit for the dust flux or mass. At larger distances, till about 100.000 km, the noise spectra were less quiet and allowed only a measure of the density and temperature of the main electron population.

The above in situ detection is based on an unconventional use of the radio receiver. Though no comet proper radioemission was detected, a conventional use was also performed whenever the cometary plasma occulted partially the galactic radio source and broadened the earth kilometeric radiation /5/. This provided informations on the large scale three-dimensional structure of the comet.

This paper discusses the physics of the measurement process, the main results obtained, and some implications for ground-based experiments.

USING A RADIO-RECEIVER TO DETECT PLASMA, MOLECULES OR GRAINS

The conventional use of a radio receiver is the detection of electromagnetic waves from remote sources. But, since electric antennas are sensitive to local electrostatic field fluctuations, they can also be used as in-situ detectors. The first question is :

What Produces Voltage Fluctuations on an Antenna, in a Cometary Environment ?

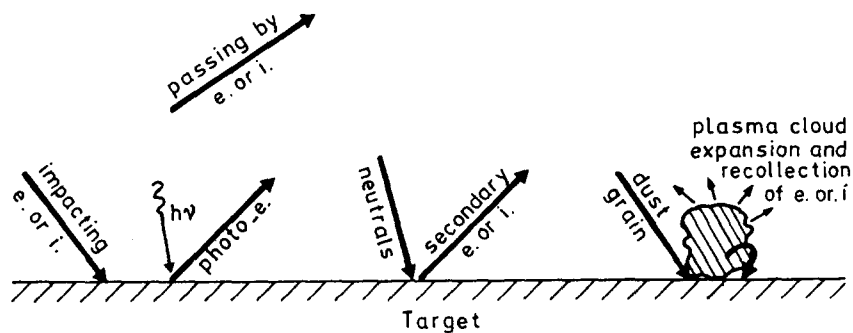


Fig. 2. Local sources of electric noise on an antenna : The relevant target is either the antenna or the spacecraft conductive surface, depending whether the antenna is in a dipole or a monopole configuration, respectively.

The answer is (Figure 2) : a) the passage of electrons or ions in the proximity of the antenna, owing to their thermal agitation and b) all other processes yielding a variation of the antenna's electric charge, namely the impacts of electrons or ions, the emission of photoelectrons due to solar irradiation, the secondary emission of electron or ions due to molecule impacts and, finally, the dust grain impacts yielding a plasma cloud, a part of which is subsequently recollected.

The former process, which is known as the plasma thermal noise (or "quasi-thermal" in the absence of thermal equilibrium), has the best diagnosis value, as illustrated in Figure 1 : a dipole sufficiently long and thin will sense the nearly unperturbed ambient plasma.

On the other hand, the latter processes depend on the number of impacting or emitted charged particles and of their trajectories, which in turn depend on both the floating d-c potential and the nature of the target through the emission yield. Another important point to be clarified is : what is the target which detects the impacts ? For a symmetric dipole antenna, the receiver measures the potential between the two arms ; thus the relevant target is the antenna surface /2/ since an impact on the conductive spacecraft's skin produces nearly the same potential on the two antenna arms. On the other hand, for a monopole antenna, the receiver detects the potential between the antenna and the spacecraft ; thus, all impacts, whether they are on the antennas or on the spacecraft are detected ; therefore, the relevant target is the spacecraft conductive skin itself since it has generally a much larger surface than the antenna.

Indeed, the ICE dipole measured mainly the plasma thermal noise, while the monopole detected mainly the plasma impact noise.

Plasma Thermal Noise

The plasma thermal noise is due to the electrostatic fluctuations associated to the natural motion of the charged particles. For calculating it, the plasma collective properties and spatio-temporal dispersion play a crucial role. First, let us consider frequencies f of the order of magnitude of the electron plasma frequency f_p . For $f < f_p$, the electrons have enough time to react, i.e. the temporal dispersion is small; since the plasma tends to be neutral, each electron is "sheathed" so that its potential does not extend farther than the Debye length L_D . Thus, a passing-by thermal electron with velocity $v_{th} \sim L_D \omega_p$ induces on the antenna a voltage pulse of duration $1/\omega_p$. This explains why the noise spectrum is "white" at low frequencies.

On the other hand, for $f > f_p$, the spatio-temporal dispersion is important and the thermal motions produce plasma waves, of wave number $k \sim (1-f^2/f_p^2)^{1/2}/L_D$. Since the antenna of length L is mostly sensitive to waves $k \sim 1/L$, the noise spectrum will have a peak just above f_p if $L/L_D \gg 1$, but would exhibit only a smooth variation around f_p for shorter antennas. This explains why this so-called "plasma line", when measured with an actual antenna /6/ is not exactly at $f = f_p$ and is not at all a "line" if $L/L_D < 1$. This simple description concerns a thermal plasma; a small quantity of suprathermal electrons (by small we mean a quantity which changes negligibly the real part of the plasma dispersion equation) will only modify the spectrum for $f \sim f_p$ since they interact with waves of phase velocity of order their proper velocity, i.e. much nearer to f_p than thermal electrons.

Thus, a plasma electron noise detector must have a frequency range including f_p and a length $L > L_D$, as was the case for the ICE dipole antenna during the comet encounter (Figure 3). In general, the calculation of the electrostatic noise power spectrum on a linear antenna (aligned with the Oz axis) involves an integration of the plasma electric field fluctuation spectrum $\langle E_z E_z \rangle_{k\omega}$ /7/, as /6, 8, 9/

$$V^2 = \frac{2}{(2\pi)^3} \int d^3k \langle E_z E_z \rangle_{k\omega} |J(\vec{k})|^2 \tag{1}$$

where $J(\vec{k})$ is the Fourier transform of the antenna current distribution, i.e. $J(\vec{k}) \sim 4 \sin^2(k_z L/2)/k_z^2 L$ for a thin wire dipole (L is the length of one arm) and $J(\vec{k}) = 2 \sin(k_z L/2)/k_z$ for a dipole consisting of two small spheres distant by L .

Equation (1) can sometimes be approximated analytically /6, 9, 10/. Table 1 shows the power spectrum V^2 in units of $10^{-14} \text{ V}^2 \text{ Hz}^{-1}$, for a plasma of temperature T (eV), density n (cm^{-3}) and an antenna length $L > L_D = 7 (T/n)^{1/2}$, as a function of the parameter $x = f/f_p$

TABLE 1 Plasma Thermal Noise

$x = f/f_p$	dipole wire antenna	dipole sphere antenna
$x < 1$	$40 T n^{-1/2} L^{-1}$	$T^{1/2}$
$x > 1 + (\frac{L_D}{L})^2$	$65 \frac{T n^{-1/2} L^{-1} x^3}{1-x^2}$	$1.5 \frac{T^{1/2} x^2}{(1-x)^{1/2}}$

The above expressions are to be modified if the ambient magnetic field is important /11/ or if a Doppler shift changes the frequency of the ion contribution to the spectrum /12/. In the presence of a small quantity of suprathermal electrons with temperature $T_H = tT$, the noise is roughly multiplied by t at the peak /8/, and by the ratio of total pressure to cold pressure at high frequencies $(\omega/\omega_p > t^{1/2})$ /6/.

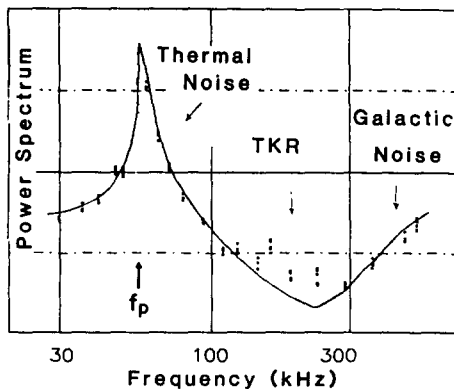


Fig. 3. Typical noise spectrum measured during the cometary encounter. The continuous line is the theoretical plasma with $n_c = 37 \text{ cm}^{-3}$, $T_c = 5.10^4 \text{ K}$, $n_H \sim 1.5 \text{ cm}^{-3}$, $T_H \sim 5.10^5 \text{ K}$; time 11 06 44 UT). The earth kilometric radiation appears sometimes near 200 kHz, while the galactic noise is above 300 kHz. The continuous horizontal line is at the $10^{-14} \text{ V}^2 \text{ Hz}^{-1}$ level at the receiver ports; the dashed-dotted lines are 10 dB apart.

Impact or Emission Noise

General expression. This noise is due to any process which transfers a charge between the antennas (or the spacecraft, in the monopole configuration) and the plasma. Each individual event produces a variation of potential $\delta V(t)$, and N independent events per unit time yield a power spectrum

$$V^2 = 2 N |\delta V(\omega)|^2 \quad (2)$$

where $\delta V(\omega)$ is the Fourier transform of $\delta V(t)$. If the events are not identical, Equation (2) has to be replaced by a sum (discrete or continuous) over the events.

What is the form of $\delta V(\omega)$? Let τ_r be the rise time of the signal $\delta V(t)$ and τ_d its decay time (Figure 4). The decay time is τ_d due to the discharge currents through both the receiver and the plasma; R and C being respectively the total resistance and capacitance of the system, it is of the form

$$\tau_d \sim RC \quad (3)$$

It is generally larger than the rise time τ_r , which depends on the dynamics of the transferred charge Q . Then, the general form of the spectrum is easily seen to be /10, 13/

$$V^2 = \frac{N Q^2}{2 C^2 \omega^2} \frac{1}{1 + \omega^2 \tau_r^2} \frac{1}{1 + \omega^2 \tau_d^2} \quad (4)$$

At frequencies $\omega = 2\pi f \ll \tau_d^{-1}$, each event is viewed by the receiver as an infinitesimal pulse, yielding a white spectrum; at intermediate frequencies $\tau_d^{-1} \ll \omega \ll \tau_r^{-1}$, each event is viewed as a step function, yielding an f^{-2} power spectrum; at high frequencies, each event is characterized by the discontinuity of its derivative in the rising part, yielding a generic f^{-4} power spectrum (Figure 4). Note that Equation (4) is exact only in these particular frequency ranges; or if the rising part has the form $(1 - e^{-t/\tau_r}) H(t)$, $H(t)$ being the unit step function; otherwise, the exact spectrum at the transition between the three regimes depends on the details of the variation $\delta V(t)$.

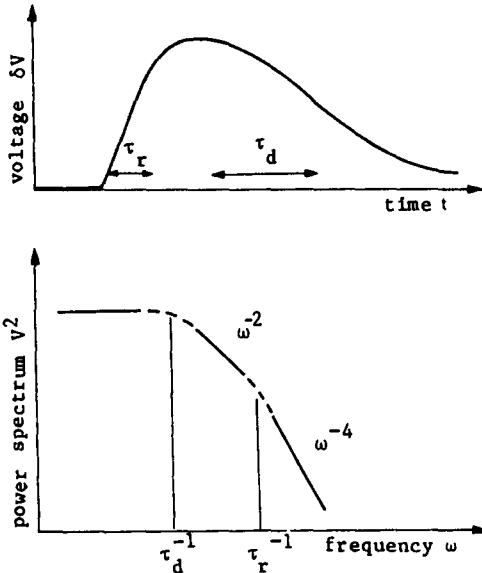


Fig. 4 Potential induced on the antenna, due a transfer of charge from (or to) the plasma, and corresponding typical spectrum at low, intermediate and high frequencies.

Now, we investigate the particular cases of plasma impacts, photoelectron emission, molecules and grains impacts.

Plasma impacts and photoelectron emission. The impact of one electron or ion yields a transfer of charge $Q \sim e$ between the plasma and the target, when the reflexion and secondary emission are small (as is the case for the particle energies considered in this paper). Likewise, a photoelectron emission produces a transfer $Q=e$.

To calculate the rise time τ_r , we note that when the charge Q is at a distance r sufficiently far from the surface, it induces a voltage small with respect to that ($\sim Q/C$) produced when it has reached it. Typically, $r \sim \text{Min}(L_D, D)$, where L_D takes account of the Debye shielding and D is the scale relevant to calculate the capacitance C ; for a wire dipole antenna of length L ($C \propto L$) $D \sim L$; for a double sphere antenna of radius a ($C \propto a$) $D \sim a$; for a monopole antenna where the target is the spacecraft of size D_S/C , $D \sim D_S/C$. Thus $\tau_r \sim r/v$ where v is the particle's velocity in the spacecraft frame.

In practice, one has generally $D > L_D$, thus $\tau_r \sim \omega_p^{-1}$ for plasma electrons.

Now, we calculate the mean number of events N . Let N_e (resp. N_i) denote the electrons (resp. ions) impact rate and N_{ph} denote the photoemission rate. If these processes are the dominant charging processes, the charge equilibrium yields $N_e - N_i = N_{ph}$. Thus $N = N_e + N_i + N_{ph} = 2 N_e$. Using standard approximate expressions for N_e (see for instance /14/), Equation (4) yields, in the particular case $\tau_d \ll \omega \ll \tau_r$ which is relevant for $f < f_p$

$$V^2 \sim 0.8 \cdot 10^{-12} \frac{S (m^2)}{C^2 (pF)} \left(\frac{f_p}{f}\right)^2 T_{(ev)}^{\frac{1}{2}} f(\phi) V^2 Hz^{-1} \quad (5)$$

where C is the antenna capacitance, S is target's surface, ϕ the ratio of its dc-potential to the electron temperature $T(ev)$ and $f(\phi)$ stands for the variation of the electron flux (for $\phi \ll 1$, $f(\phi) \sim 1$; if $\phi < 0$ $f(\phi) \sim e^{\phi}$). Using standard expressions of the antenna capacitance, we obtain for V^2 (in units of $10^{-14} V^2 Hz^{-1}$), for wire and spherical dipole antennas of radius a , assuming $f(\phi) \sim 1$ and $x = f/f_p < 1$, the following values /10/

TABLE 2 Plasma Impact and Emission Noise

dipole wire antenna	dipole sphere antenna
$2.2 \frac{a}{L} (\ln(\frac{a}{L_D}))^2 T^{\frac{1}{2}} x^2$	$T^{\frac{1}{2}} x^2$

For a monopole antenna, one must return to Equation (5) where S is the equivalent collecting spacecraft surface. Since the capacitance is roughly two times the dipole one, the expression in Table 2 should be multiplied by 0.25 times the ratio of the spacecraft and antenna collecting surfaces. Comparing Table 1 and 2, one sees that the noise due to plasma impacts is in practice much smaller than the thermal noise near the plasma frequency for a dipole wire antenna. This is not the case for a double sphere antenna, nor for a monopole.

Figure 5 shows an application of these results to the ICE encounter with comet Giacobini-Zinner. For the wire dipole antenna, the plasma impact or emission noise is negligible with respect to the thermal noise except in the cold dense plasma sheet. On the other hand, for the monopole antenna it is everywhere important; from its amplitude, we deduce that the spacecraft floating potential, which was positive in the solar wind, became $\sim -2 V$ in the dense plasma sheet.

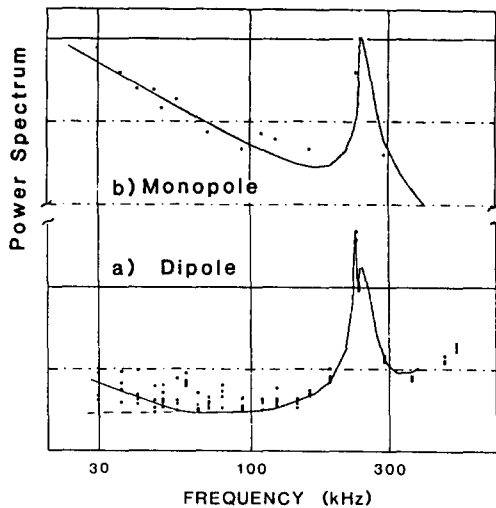


Fig. 5 Noise spectrum measured near closest approach (11 02 32 UT) on respectively the dipole (a) and monopole (b) antenna. The continuous line is the theoretical plasma thermal and impact noise giving the best fit to the results (bimaxwellian plasma with $n_c = 670 cm^{-3}$, $T_c = 1.7 \cdot 10^4 K$, $n_H \sim 20$, $T_H \sim 1.7 \cdot 10^5 K$). a) On the dipole, the noise is mainly quasi-thermal, except at very low frequencies; the dashed line corresponds to the antenna pointing in the sun direction: then, the photoelectron current is negligible, yielding a negative potential, thus $f(\phi) \ll 1$, and the impact and emission noise is negligible (Equation (5)). b) On the monopole, which is always perpendicular to the sun direction, the noise is mainly due to plasma impact and emission, producing an f^{-2} power spectrum (Table 2) for $f < f_p$; the best fit yields a spacecraft potential of order $-2 V$.

Molecules impacts. Molecules high-velocity impacts produce a secondary emission of electrons and ions. This has two main consequences. First, since the yields for secondary emission of electrons (γ_e) and ions (γ_i) are generally not equal, this modifies the current balance equation; thus the spacecraft or antenna floating potential changes, which changes in turn the plasma impact and emission noise calculated above. Second, these secondary electrons and ions produce themselves a noise; its general expression is given by Equation (4), with $Q=e$ and $N = \gamma_{e,i} N_G$ (if $\gamma_{e,i} < 1$) where N_G is the molecule impact rate.

This effect is very important for the Giotto and Vega encounters with Halley, owing to the high molecule impact rate and kinetic energy (see /15/). Let us calculate it for the ICE/G-Z encounter. First, taking a molecular production rate $Q \sim 3 \cdot 10^{28} \text{ s}^{-1}$ /16/ and a 21 km/s velocity, and using the plasma parameters measured aboard ICE /2, 3/, we find that the molecular (N_G) and electron (N_e) impact rates satisfy $N_G/N_e < 10 / f$ (ϕ).

Second, the molecule kinetic energy in the spacecraft frame is too small (2 eV amu^{-1}) for kinetic emission to occur /17/, so that γ is negligible; the yield γ_1 , due to sputtering, is expected to be $\gamma_1 < 2 \cdot 10^{-3}$ /18/. Thus, we find $\gamma_{e,1} N_G/N_e \ll 1$ so that the effect of molecules impacts is negligible, both on the floating potential and on the noise.

Dust impacts. When a small dust grain hits the spacecraft or antennas with high velocity, it is vaporized and ionized, as also a small part of the target's material. This produces an expanding plasma cloud, and a fraction Q of the released charge is recollected. The general expression of the noise is still given by Equation (4) where N is the grain impact rate on respectively the antennas (in dipole configuration) or the spacecraft (in monopole configuration).

The charge released is a function of the grain mass m and velocity v , and of the target and grain materials. This problem has been extensively studied in the frame of in-situ dust detectors and yields a variation of the form $Q \sim Q_0 m^\alpha v^\beta$ with $\beta \sim 3.5$ and $0.6 < \alpha < 1$. An order of magnitude /19/ for ICE parameters is

$$Q \text{ (Cb)} \sim A 10^{-2} m^{0.8} \quad (6)$$

where $A < 1$ stands for the proportion of the released charge that is recollected.

Let us now evaluate the time scales τ and τ_d in Equation (4). The decay time τ_d of the signal produced by an impact is still given by Equation (3). On the other hand, the rise time τ depends on the dynamics of the plasma cloud expansion and charge recollection (see /20/). It can be estimated by simple physical considerations /13/. In particular, it must be smaller than the time taken by the diameter of the expanding cloud to reach the target's smallest size i.e. $\tau < D/2 v_{ex}$, where $D = a$ (antenna radius) in dipole configuration or $D = D_S/C$ (spacecraft size) in monopole configuration, and v_{ex} is the cloud expansion velocity ($\sim 10 \text{ km/s}$ for ICE). Other constraints are studied in the Meyer-Vernet et al./13/ paper; in particular, it should be smaller than the time taken by the plasma density in the cloud to decrease to the ambient level.

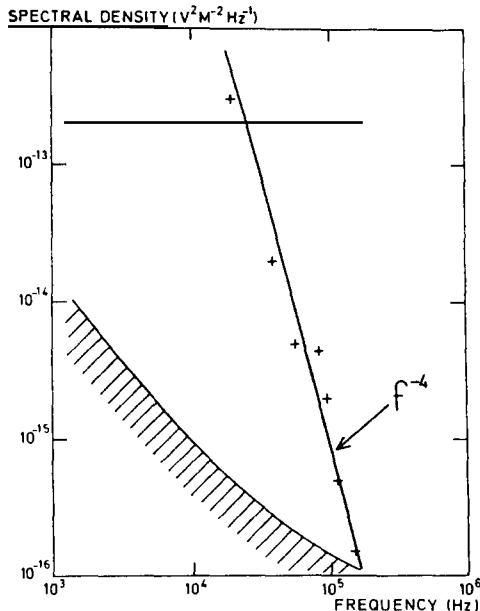


Fig. 6 Noise power spectrum measured by the Planetary Radio Astronomy instrument aboard Voyager at Uranus ring plane crossing. This noise is interpreted as due to grain impacts on the spacecraft and has provided dust parameters /13/. The spectrum is in f^{-4} because the frequency range is much higher than the inverse of the rise time of the signal due to each individual impact (see Fig.4) (from /13/).

The corresponding spectra, with the generic form as given in Equation (4) and Figure 4, have

indeed been measured by the Planetary Radio Astronomy experiment on Voyager 2 at respectively Saturn /21/ and Uranus /13/ ring plane crossing, (Figure 6), and by the Plasma Wave Instrument /22/ on the ICE/GZ encounter.

Fitting the observations with Equation (4) yields the quantity NQ^2 which is in fact (using Equation (6)) a mean over the grains mass distribution.

$$NQ^2 \sim A^2 10^{-4} S_{\perp} v \int^{m_{\text{Max}}} dm \frac{dn_G}{dm} m^{1.6} \quad (7)$$

where S_{\perp} is the target's projected surface, dn_G/dm is the number (per unit volume) of grains of mass between m and $m + dm$, and m_{Max} is the mass of the largest grains which have been collected during the time intervall where the noise spectrum has been acquired.

APPLICATION : UPPER LIMIT ON THE DUST

During the 20 minutes quiet tail crossing, the data fit almost perfectly the theoretical plasma noise spectra. Using Equations (4) and (7) and taking account of the dead time, this yields an upper limit on the dust in this region /2/. To obtain a conservative estimate, we use $A \sim 0.1$. The measurements with the two different antennas, i.e. dipole with $S_{\perp} \sim 3.5 \cdot 10^{-2} \text{ m}^2$ (projected surface of the dipole antenna) and monopole with $S_{\perp} \sim 3.2 \text{ m}^2$ (total projected surface of the spacecraft), yield two independent limits.

We find in particular that the mean dust concentration, between 7800 and 15,000 km from the comet nucleus, was smaller than 10^{-5} m^{-3} for grains of mass $m > 10^{-10} \text{ g}$ (i.e. radius $> 3 \mu\text{m}$ if the density is 1 g cm^{-3}) or $2 \cdot 10^{-3} \text{ m}^{-3}$ for grains of mass $m > 4 \cdot 10^{-12} \text{ g}$ (i.e. radius $> 1 \mu\text{m}$ if the density is 1 g cm^{-3}).

Now, we compare these figures with those derived from the plasma wave instrument /22/. These authors do not decide whether the target for the impacts is the antenna or the spacecraft. However, since their antenna is a symmetric dipole, the relevant target is expected to be the antennas, except if the receiver system is itself disymmetric; in the latter case, the amplitude detected would depend on this disymmetry and the interpretation of the results would be rather unreliable. Thus, let us assume that their target is the antenna. They detect grains with mass between $4 \cdot 10^{-12}$ and 10^{-10} g , and their limit yields a grain mean number density which is a little below our upper limit, thus perfectly compatible with it.

On the other hand, our figures are clearly incompatible with the results derived from infrared imaging /23/. Note that the results from the plasma wave instrument are also incompatible with the infrared results (since the compatibility would require, in the most favorable case, that the detected grains be $\sim 16 \mu\text{m}$ /23/ while the actual figures are ~ 1 to $3 \mu\text{m}$ /22/).

This incompatibility between both ICE results on one hand and ground-based results on the other hand, suggests that either the impact ionization figures such as Equation (6) (and a similar one used for interpreting the Plasma wave instrument data) are grossly overestimated, or the grain model used for interpreting the infrared data is itself erroneous and/or the grain density is much smaller than 1 g cm^{-3} . Indeed, the recent encounters with Halley have shown that the dust models need important modifications /24, 25/; in addition, comet Giacobini-Zinner has been suggested from long time to have feather-like grains with density much smaller than 1 g cm^{-3} .

APPLICATION : PLASMA MEASUREMENTS

In the quiet plasma tail, the spectra measured on the dipole antenna fit almost perfectly (Figure 3) the plasma thermal noise calculated /9/ with a bi-maxwellian electron velocity distribution defined by the parameters n_c , n_H (cold and hot electron density), T_c , T_H (cold and hot electron temperature). The hot population contributes always by less than 10 % to the total electron density; in most cases, it is a few percent. Its temperature is between 3 and 100 times the cold temperature /2, 3/. (Note that a warmer tail of the electron velocity distribution would not be detectable with our frequency resolution, except if it would contribute in an important way to the total electron pressure).

In practice, the fitting yields easily the total electron density ($n_c + n_H$), the cold electron temperature (T_c) and the total pressure ($\alpha(n_c T_c + n_H T_H)$). The separate determination of n_H and T_H is less precise since it requires a good frequency resolution in the peak of the spectrum, which is not always achieved.

Note also that, since the antenna length is much larger than both the spacecraft scales (Figure 1) and the Debye lengths of the cometary plasma and the secondary plasma, we are sure that we are detecting the cometary plasma itself. This configuration is especially useful in the comet plasma tail because i) the comet electron temperature is of the same order as that of the photoelectrons emitted by the spacecraft (1 to 2 eV), ii) the comet electron bulk velocity in the spacecraft frame is low,, and iii) the photoelectrons density near the spacecraft is expected to be greater than 100 cm^{-3} , i.e. of the same order of magnitude as the cometary plasma, so that the two populations cannot be safely distinguished by ordinary sensors located near the spacecraft skin.

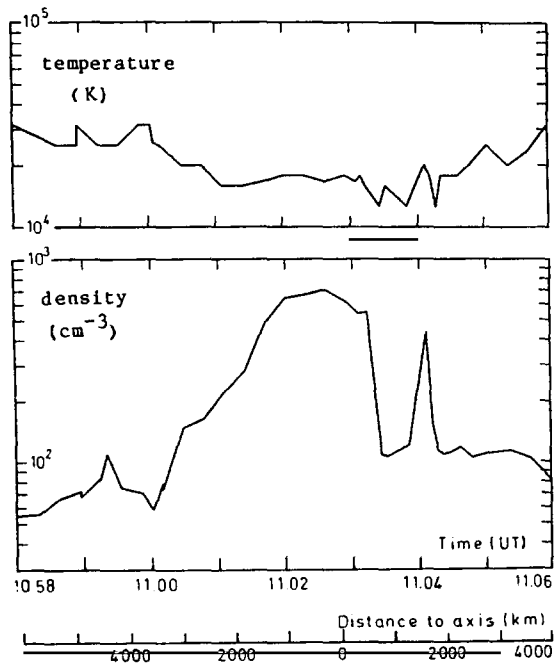


Fig. 7 Electron density and temperature measured near closest approach by thermal noise spectroscopy with a bi-maxwellian distribution. The density is the total density ($n_c + n_h$) while the temperature is that of the cold population (T_c). In the dense plasma sheet, the other population has mean parameters $n_h \sim 15 \text{ cm}^{-3}$, $T_h \sim 10 \text{ eV}$. The spacecraft crossed the aberrated tail axis near 11.02.45 UT and the distance plotted is along the S/C trajectory (which was South-North at 20.7 km/s) in the comet's frame.

Figure 7 shows an expanded view of the total electron density and cold electron temperature deduced in the central region /2, 3/. The $\sim 1500 \text{ km}$ (along ICE trajectory) wide region where the density remains above 600 cm^{-3} /2, 3/, (the maximum value being 700 cm^{-3}) corresponds to the low ($\sim 5 \text{ nT}$) magnetic field sheet separating the magnetic lobes of opposite polarity /26/. Owing to the orientation of this plasma sheet at encounter time /26/, this corresponds to a true width $\sim 800 \text{ km}$.

In this region, the cold electron temperature remains constant at 1.4 eV. On the other hand, we find a more variable warm population, near density 15 cm^{-3} and temperature 10 eV. This population contributes negligibly to the electron pressure, except in $\sim 5000 \text{ km}$ on both sides of the plasma sheet, i.e. in the tail magnetic lobes; this could suggest /3/ heating processes possibly due to a viscous-like interaction with the solar wind /27/. The two density peaks less than 500 km wide on each side of the plasma sheet suggest either cometary rays or dynamic phenomena.

Figure 8 shows the same parameters plotted in a wider region as a function of the distance R to the comet's nucleus /3/. A striking point is that the density decreases rather abruptly in the tail magnetic lobes on both sides of the plasma sheet, and then varies as R^{-2} for $R < 20,000 \text{ km}$ /3/, while the temperature varies as R^{-3} . This R^{-2} variation of the density, which we find outside the region where the ions and neutrals are collisionally coupled, has also been found by the Giotto Ion Mass Spectrometer in comet Halley outside the contact surface /28/.

The 100 % fluctuations of both the density and temperature that we observe outside $R \sim 20,000 \text{ km}$, have been also found by other experimenters /4/; this region has been termed the "sheath" /4/.

These in-situ results concern a linear cut of the comet's tail nearly perpendicular to its axis. This is at variance to earth-based measurements which generally involve an integration

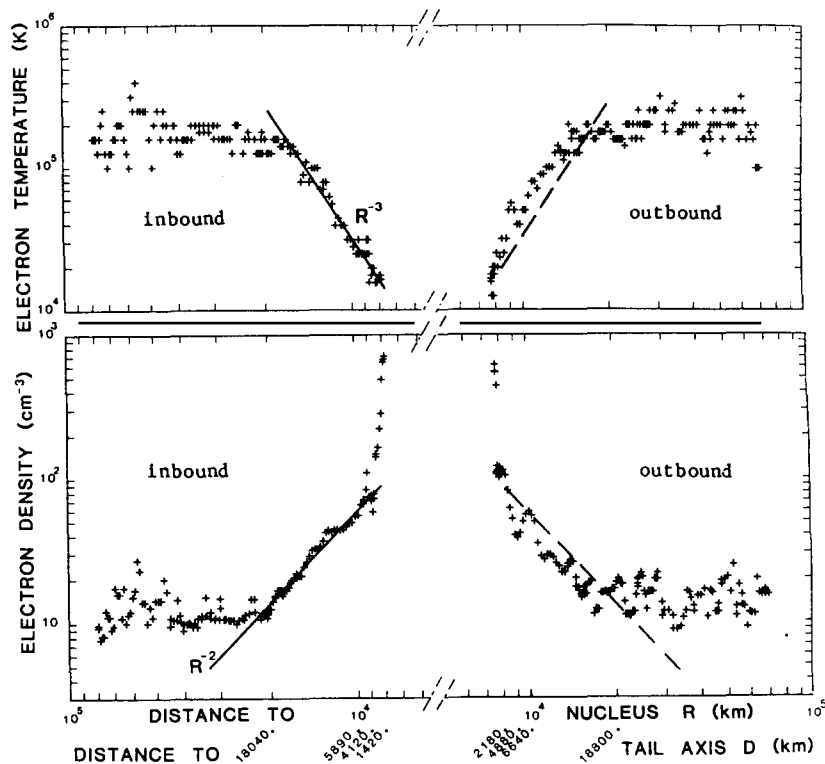


Fig. 8 Electron density and temperature as a function of the distance to the comet's nucleus. (The distance to the aberrated tail axis is shown at the bottom). The continuous lines are R^{-2} and R^{-3} variations for the inbound trajectory; the dashed lines are their symmetrical on the outbound side, showing a slight disymmetry (from /3/).

over the comet's 3-Dimensional structure. By using our electron density measurements in the plasma sheet and the coma R^{-2} region, we can estimate the integrated electron density. The resulting profile, which amounts to $\sim 3 \cdot 10^{11}$ electrons/cm² at closest approach can interpret an H_2O^+ emission profile measured during the encounter /29/: the comparison of both profiles gives important hints on the comet's structure; in particular, it yields a ratio of H_2O^+ column density to total ion column density $\sim 1:5$ /30/.

A CONVENTIONAL USE OF THE RADIO-RECEIVER

The most important results obtained with the radio receiver during the comet's encounter stem from the unconventional use described above. However, though no comet's proper radio emission was recorded, a conventional use was performed when the comet occulted both the galactic and earth radio sources /5/. The interpretation of the galactic source occultation showed that the 3-dimensional large scale structure of the coma is consistent with the structure determined from in-situ measurements made along the trajectory. The earth radio source occultation showed that the large plasma density fluctuations measured by ICE in the comet's sheath along its trajectory exist also with similar properties in the perpendicular direction /5/.

REFERENCES

1. R. Knoll, G. Epstein, S. Hoang, G. Huntzinger, J.L. Steinberg, J. Fainberg, F. Grena, S.R. Mosier, and R.G. Stone, The 3-dimensional radio mapping experiment (SBH) on ISEE-C, *IEEE trans.*, GE-16, 199 (1978).
2. N. Meyer-Vernet, P. Couturier, S. Hoang, C. Perche, J.L. Steinberg, J. Fainberg, and C. Meetre, Plasma diagnosis from thermal noise and limits on dust flux or mass in comet Giacobini-Zinner, *Science*, 232, 370 (1986).
3. N. Meyer-Vernet, P. Couturier, S. Hoang, C. Perche, and J.L. Steinberg, Physical parameters for hot and cold electron populations in comet Giacobini-Zinner with the ICE radio experiment, *Geophys. Res. Lett.*, 13, 279 (1986).
4. S.J. Bame, R.C. Anderson, J.R. Asbridge, D.N. Baker, W.C. Feldman, S.A. Fuselier, J.T. Gosling, D.J. McComas, M.F. Thomsen, D.T. Young, and R.D. Zwickl, Comet Giacobini-

- Zinner : Plasma description, Science, 232, 356 (1986).
5. J.L. Steinberg, J. Fainberg, N. Meyer-Vernet, and S. Hoang, Broadening and occultation of radio sources by comet Giacobini-Zinner as observed from ICE, Geophys. Res. Lett., 13, 407 (1986).
 6. N. Meyer-Vernet, On natural noises detected by antennas in plasmas, J. Geophys. Res. 84, 5373 (1979).
 7. A.G. Sitenko, Electromagnetic Fluctuations in Plasma, Academic, New-York, 1967.
 8. J.A. Fejer and J.R. Kan, Noise spectrum received by an antenna in a plasma, Radio Sci., 4, 721 (1969).
 9. P. Couturier, S. Hoang, N. Meyer-Vernet, and J.L. Steinberg, Quasi-thermal noise in a stable plasma at rest : theory and observations from ISEE 3, J. Geophys. Res., 86, 11127 (1981).
 10. N. Meyer-Vernet, Quasi-thermal noise corrections due to particle impacts or emission, J. Geophys. Res., 88, 8081 (1983).
 11. D.D. Sentman, Thermal fluctuations and the diffuse electrostatic emissions, J. Geophys. Res., 87, 1455 (1982).
 12. N. Meyer-Vernet, P. Couturier, S. Hoang, J.L. Steinberg, and R.D. Zwickl, Ion thermal noise in the solar wind : interpretation of the "excess" electric noise on ISEE 3, J. Geophys. Res., 91, 3294 (1986).
 13. N. Meyer-Vernet, M.G. Aubier, and B.M. Pedersen, Voyager 2 at Uranus : grain impacts in the ring plane, Geophys. Res. Lett., in press (1986).
 14. J.G. Laframboise and L.W. Parker, Probe design for orbit-limited current collection, Phys. Fluids, 16, 629 (1973).
 15. R.J.L. Grard, Shot noise generated by gas impact during a cometary fly-by, in : Spacecraft/Plasma interactions, ESA SP-198, ESTEC, Noordwijk, The Netherlands 1983, p. 151.
 16. L.A. Mc Fadden, M.F. A'Hearn, P.D. Feldman, H. Böhnhardt, J. Rahe, M.C. Festou, J.C. Brandt, S.P. Maran, M.B. Niedner, A.M. Smith, and D.G. Schleicher, Ultraviolet spectrophotometry of comet Giacobini-Zinner during the ICE encounter, Geophys. Res. Lett., in press (1986).
 17. D.T. Young, Secondary ions and electrons emitted by Giotto, in : Spacecraft/Plasma interactions, ESA SP-198, ESTEC, Noordwijk, The Netherlands 1983, p. 143.
 18. D.T. Young, Spacecraft environment during the Giotto-Halley encounter : a summary, in : The Giotto spacecraft Impact-Induced Plasma environment, ESA SP-224, ESTEC, Noordwijk, The Netherlands, 1984, p. 99.
 19. F.R. Krüger and J. Kissel, Experimental investigations on ion emission with dust impact on solid surfaces, in : The Giotto spacecraft Impact-Induced plasma environment, ESA SP-224, ESTEC, Noordwijk, The Netherlands, 1984, p. 43.
 20. H. Maassberg, A model of plasma cloud expansion generated by a dust particle impact, in : The Giotto spacecraft Impact-Induced plasma environment, ESA SP-224, ESTEC, Noordwijk, The Netherlands, 1984, p. 59.
 21. M.G. Aubier, N. Meyer-Vernet, and B.M. Pedersen, Shot noise from grain and particle impacts in Saturn's ring plane, Geophys. Res. Lett., 10, 5 (1983).
 22. D.A. Gurnett, T.F. Averkamp, F.L. Scarf, and E. Grun, Dust particles detected near Giacobini-Zinner by the ICE plasma wave instrument, Geophys. Res. Lett., 13, 291 (1986).
 23. H. Campins, C.M. Telesco, R. Decher, D. Mozurkewich, and H.A. Thronson, Jr., Groundbased infrared imaging of comet Giacobini-Zinner : The distribution of dust during the ICE flyby, Geophys. Res. Lett., 13, 295 (1986).
 24. R.Z. Sagdeev, J. Blamont, A.A. Galeev, V.I. Moroz, V.D. Shapiro, V.I. Shevchenko, and K. Szegö, Vega spacecraft encounters with comet Halley, Nature, 321, 259 (1986).
 25. R. Reinhard, The Giotto encounter with comet Halley, Nature, 321, 313 (1986).
 26. J.A. Slavin, E.J. Smith, B.T. Tsurutani, G.L. Siscoe, D.E. Jones, and D.A. Mendis, Giacobini-Zinner magnetotail : ICE magnetic field observations, Geophys. Res. Lett., 13, 283 (1986).
 27. H. Perez-de-Tejada, private communication (1986).
 28. H. Balsiger, K. Altwegg, F. Bühler, J. Geiss, A.G. Ghielmetti, B.E. Goldstein, R. Goldstein, W.T. Huntress, W.H. Ip, A.J. Lazarus, A. Meier, N. Neugebauer, U. Rettenmund, H. Rosenbauer, R. Schwenn, R.D. Sharp, E.G. Shelley, E. Ungstrup, and D.T. Young, Ion composition and dynamics at comet Halley, Nature, 321, 330 (1986).
 29. M.A. Strauss, P.J. McCarthy, and H. Spinrad, Optical spectrophotometry of comet P/Giacobini-Zinner and emission profiles of H_2O^+ , Geophys. Res. Lett., 13, 389 (1986).
 30. N. Meyer-Vernet, M.A. Strauss, J.L. Steinberg, and H. Spinrad, in preparation (1986).

Acknowledgements. The ISEE 3/ICE radio experiment is a joint project of the CNRS UA 264 at Paris Observatory and the LEP at NASA/GSFC. J.L. Steinberg was Principal Investigator. The team which reduced and interpreted the results of the comet encounter included also P. Couturier, S. Hoang, and C. Perche at Paris Observatory, and J. Fainberg and C. Meetre at NASA/GSFC. The success was largely due to the high sensitivity of the receiver which was constructed by a team led by R. Knoll, in France and USA under contract with C.N.E.S.